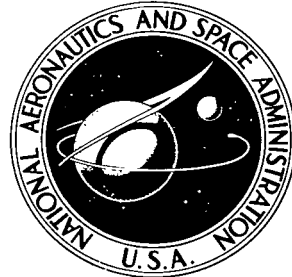


NASA TECHNICAL NOTE

NASA TN D-6441



NASA TN D-6441
C. I



TECH LIBRARY KAFB, NM

LOAN COPY: RETURN
AFVWL (DO4L)
KIRTLAND AFB, N. M.

A METHOD FOR CALCULATING
THE AERODYNAMIC LOADING ON
WING-BODY COMBINATIONS AT
SMALL ANGLES OF ATTACK
IN SUPERSONIC FLOW

by Charlie M. Jackson, Jr., and Wallace C. Sawyer
Langley Research Center
Hampton, Va. 23365

NATIONAL AERONAUTICS AND SPACE ADMINISTRATION • WASHINGTON, D. C. • OCTOBER 1971



0132939

1. Report No. NASA TN D-6441	2. Government Accession No.	3. Recipient's Catalog No.	
4. Title and Subtitle A METHOD FOR CALCULATING THE AERODYNAMIC LOADING ON WING-BODY COMBINATIONS AT SMALL ANGLES OF ATTACK IN SUPERSONIC FLOW		5. Report Date October 1971	
7. Author(s) Charlie M. Jackson, Jr., and Wallace C. Sawyer		6. Performing Organization Code	
9. Performing Organization Name and Address NASA Langley Research Center Hampton, Va. 23365		8. Performing Organization Report No. L-7822	
12. Sponsoring Agency Name and Address National Aeronautics and Space Administration Washington, D.C. 20546		10. Work Unit No. 720-01-11-01	
15. Supplementary Notes		11. Contract or Grant No.	
		13. Type of Report and Period Covered Technical Note	
		14. Sponsoring Agency Code	
16. Abstract This report describes a theoretical method for estimating the aerodynamic loading on a wing-body configuration. In order to provide a basis for evaluation of the method, experimental measurements of surface pressures, forces, and moments were made on a series of basic wing-body configurations over a Mach number range from 2.5 to 4.5. Comparison of the theoretical estimates with these experimental data generally indicated good agreement for the entire range of configurations and test conditions.			
17. Key Words (Suggested by Author(s)) Missile aerodynamics Aerodynamic prediction techniques Wing-body interference		18. Distribution Statement Unclassified – Unlimited	
19. Security Classif. (of this report) Unclassified	20. Security Classif. (of this page) Unclassified	21. No. of Pages 32	22. Price* \$3.00

**A METHOD FOR CALCULATING THE AERODYNAMIC LOADING
ON WING-BODY COMBINATIONS AT SMALL ANGLES OF
ATTACK IN SUPERSONIC FLOW**

By Charlie M. Jackson, Jr., and Wallace C. Sawyer
Langley Research Center

SUMMARY

A theoretical method has been developed for estimating the aerodynamic loading on wing-body configurations at supersonic speeds and small angles of attack. The method uses second-order shock-expansion theory for the body effects and linear theory for the wings. In order to provide a basis for evaluation of the theoretical method, experimental measurements of surface pressure were made at selected survey positions on each of a series of basic wing-body configurations over a Mach number range from 2.5 to 4.5 and at angles of attack up to 6° . Force and moment measurements were also made for this same series of models at these test conditions. Comparison of the theoretical estimates with the experimental data generally indicated good agreement for the entire range of configuration and test variables. The agreement demonstrated by this comparison indicates that reliable preliminary design estimates can be obtained for the detailed aerodynamic loading as well as the longitudinal aerodynamic stability and control of complete wing-body configurations.

INTRODUCTION

Early in the design phase of aircraft or missile development programs it is necessary to have estimates of the aerodynamic loading for the entire supersonic flight regime. In the low supersonic speed range there are currently available several theoretical methods for determining the aerodynamic loading of aircraft configurations (refs. 1 to 3). These methods, which are based on supersonic linearized theory, are capable of giving adequate estimates of the aerodynamic loading provided the linearity assumptions are not violated. Generally, the methods have been shown to be applicable at speeds up to about Mach 3 for vehicles designed with emphasis on supersonic cruise efficiency (the supersonic transport configuration and many bomber and fighter airplanes).

However, in a number of instances, especially for missile configurations, the speed and volumetric limitations of the linearized theory are exceeded to such a degree that the methods are of questionable value.

References 4 and 5 have provided an initial step toward developing analytical methods for the prediction of aerodynamic loading on configurations for which the linear-theory assumptions are violated. The present paper presents the analytical methods of references 4 and 5 and an extension of these methods to provide lifting effects on the aerodynamic loading of wing-body configurations. These analytical methods are evaluated by comparison with experimental surface pressures, forces, and moments for several configurations.

In the formulation of the method presented in this paper, the surface pressures on the body and the wing are estimated with second-order shock-expansion and linear-theory wing solutions, respectively. First-order interference effects are obtained by superimposing the wing and body flow fields.

SYMBOLS

A	reference area (body maximum cross-sectional area)
C_A	axial-force coefficient, $\frac{\text{Axial force}}{qA}$
C_m	pitching-moment coefficient, $\frac{\text{Pitching moment}}{qAl}$
C_N	normal-force coefficient, $\frac{\text{Normal force}}{qA}$
$C_{N\alpha}$	slope of normal-force curve with angle of attack, $\frac{\partial C_N}{\partial \alpha}$
C_p	pressure coefficient, $\frac{(\text{Local static pressure}) - (\text{Free-stream static pressure})}{q}$
ΔC_p	lifting-pressure coefficient, $C_{p,\text{lower}} - C_{p,\text{upper}}$
c	wing chord
l	body length
M	free-stream Mach number
q	free-stream dynamic pressure
r	body radius
t/c	wing thickness ratio

X,Y,Z	Cartesian axis system (fig. 1)
x,y,z	Cartesian coordinates
x'	longitudinal coordinate, origin at wing leading edge
x_{cp}	coordinate of longitudinal center of pressure
α	angle of attack

THEORETICAL METHOD

The method to be presented for the calculation of surface pressures on wing-body configurations is formulated especially for pointed bodies of revolution with low-fineness-ratio noses and relatively thin wings. The configurations are also assumed to be vertically symmetric about the body center line in the XY- and XZ-planes. The angle of attack is assumed to be small so that the lifting and nonlifting solutions can be considered separately. A theory appropriate to bodies of revolution with low fineness ratios is applied to the body to obtain the surface pressures at zero-lift conditions and the variation of body surface pressure with angle of attack at near-zero-lift conditions. A thin-wing theory is applied to obtain the wing-induced pressures at zero lift and at low lift coefficients. The wing-body interactions are accounted for in the zero-lift conditions by superimposing the wing-induced and body-induced flow fields.

For lifting conditions, the wing is considered to be basically a thin flat plate. The influence of the body upwash field on wing loadings and the carryover of wing lift on the body are also taken into account.

Zero-Lift Solution

The theoretical methods applied to the wing-body combination to obtain the surface pressures are selected especially for the conditions of a body of revolution with a relatively low fineness ratio and thin wings. A typical configuration is depicted in figure 1(a). Since the body is assumed to be the major contributor to the flow disturbance, a high-order theory is necessary for the analysis of the body flow field. A modified form of the second-order shock-expansion theory of reference 6 was used to calculate the body surface-pressure distribution and body-induced flow-field pressures.

The wing-induced pressure field is based on the method of supersonic sources as applied to thin wings in reference 7. The application of this method requires the geometric interpretations of the configuration as illustrated in figures 1(b) and 1(c).

Figure 1(b) illustrates the mathematical model of the body required by the second-order shock-expansion theory in which the basic approach is to consider the body to be composed of many cone frustums. Starting conditions are provided on the initial cone surface by the conical flow parameters, and as the calculation proceeds downstream, a Prandtl-Meyer expansion or an oblique-shock compression is used at the frustum junctions. In order to establish the variation of flow conditions over the frustum, a series is defined to allow the initial pressure on the frustum to approach conical pressure as the frustum becomes infinitely long. This basic method and the modifications used to evaluate the body flow field are presented in detail in reference 4, along with comparisons of the theoretical results with experiment for a wide range of body shapes and flow conditions. In general, reference 4 indicates very good accuracy of the surface-pressure estimates at all conditions and a reasonably good representation of the flow-field pressures and shock shape for the bodies with lower fineness ratios.

The longitudinal pressure distribution calculated for the body alone is shown above the body in figure 1(b). The interference effects of the body on the wing are indicated by the pressure distribution on a streamwise survey line taken through the wing. The body-induced pressures are superimposed on the fin surface to provide part of the body-wing interference effect. The remaining part of the body-wing effect is accounted for by establishing flow conditions other than free stream for the wing calculations. It is assumed that the wing is embedded in a homogeneous flow field having the flow properties of the body-induced flow field at the centroid of the exposed wing planform. The Mach number at this point is obtained from the local pressure of the body flow field and the assumption that the total pressure behind the starting-cone shock is constant over the entire body flow field.

The theoretical treatment of the wing is based on the method of supersonic sources as applied to thin wings in reference 7. In the analysis presented in this paper, the wing-induced pressures are considered only in the plane of the wing. Figure 1(c) illustrates the portion of the configuration geometry used to calculate the wing-induced effects. The exposed wing panels are represented in a potential flow field as line sources and sinks according to the theory of reference 7. The pressure distributions which result from these sources and sinks in the XY-plane are also shown in figure 1(c). The wing surface pressures are represented along a wing survey line and are shown directly below the wing. The effects of the wing panels on the body are represented both along the body center line and a body meridian line in the wing plane. The corresponding pressure distributions are shown in figure 1(c) above and to the side of the body, respectively. In the present analysis the pressure distribution calculated for the body center line is assumed to be the distribution along the body vertical meridian (XZ-plane). The wing-induced pressure distributions along the body meridians between the wing plane and the vertical plane are obtained by linear interpolation. This technique is discussed and evaluated in reference 5. In order to be consistent with the assumption that the wing is embedded in the body flow field,

the wing-induced pressure field is corrected for the difference in dynamic pressure between the free stream and the body-generated flow field at the centroid of the fin.

Lifting Solution

The basic approach to the estimation of the lift-induced pressures on a wing-body combination is essentially the same as that used for the zero-lift effects in that separate theories are used and first-order interference effects are included. The second-order shock-expansion theory of reference 6 is used to obtain the lifting pressures on the body alone at small angle of attack. The lifting pressures induced by the wing are evaluated by the numerical solution to linear-theory integral equations of reference 8. These equations relate the local surface slope at a point on the lifting surface to the pressure differential at the point and the influence of the pressures upstream of the point. The numerical solution of these equations is effected by treating the wing planform as a composite of elemental rectangles and applying summation techniques to satisfy the necessary integral relations. The integral relations and the numerical techniques are discussed in detail in reference 8.

The application of the existing theoretical methods to an example wing-body configuration is illustrated in figure 2. The geometry required for the second-order shock-expansion analysis of the body is described in figure 2(b), and the geometric model required for the linear-theory analysis of the wing and interference effects is represented in figure 2(c).

The differential-pressure variation (lower-surface pressure minus upper-surface pressure) along a body of revolution at small angle of attack is obtained from the second-order shock-expansion method of reference 6 by evaluating the variation of the slope of the elemental normal-force curve with angle of attack along the body length and assuming a cosine variation of the differential pressures from the XY body meridian to the XZ meridian. The lift-curve slope and center-of-pressure estimates obtained by using this method are compared with experimental data at near zero angle of attack in reference 6 with very good results. Figure 2(b) illustrates a typical longitudinal differential-pressure variation for the body of the example configuration at small angle of attack.

The lifting-pressure effects to be calculated by the solution to linear-theory equations are illustrated in figure 2(c). These effects are the lifting pressures generated on the wing by the incidence of the wing to the flow direction, the lifting pressures generated by the wing on the body, and the body upwash effects on the wing. Since the linear-theory methods of reference 8 assume that the lifting-pressure effects are generated by a planar planform with a distribution of surface slopes to the flow, it is necessary to represent the lifting-pressure effects by this distribution of surface slope.

In the example case, a flat wing is represented in the mathematical model of figure 2(c) as a twisted and cambered wing at incidence. The slope of the wing panel at any point on the wing can be expressed as

$$\frac{\partial z}{\partial x} = \tan \alpha + \frac{r^2}{y^2} \tan \alpha \quad (1)$$

The first term of equation (1) represents the physical angle of attack of the wing and the second term represents the effect of body upwash on the wing surface. The body upwash term is presented in reference 1 and represents the upwash angle at the horizontal plane of symmetry for an infinitely long circular cylinder. The lifting pressures induced by the wing panels on the body are accounted for in the present method by including the body planform in the analysis and setting its surface slope $\frac{\partial z}{\partial x}$ equal to zero. In this way the planform of the body can receive the pressure influence of the wing panels but does not directly disturb the wing panel flow.

By using the techniques just described and superimposing the results illustrated for the body alone in figure 2(b) on the wing and interference results in figure 2(c), the differential-pressure distribution resulting from angle of attack can be obtained for the complete configuration.

NUMERICAL METHODS

The theoretical solutions discussed in the previous section have been programmed for digital computation. Because of the different techniques required for the lifting and non-lifting solutions, separate programs were written for these conditions. The inputs required to describe the geometry of the configuration were made compatible with both these programs.

The computer program used to calculate the nonlifting solution is referred to as the MISDRAG program and is presented as program DRAG in reference 5 along with the necessary operating details. The MISDRAG program includes the procedure necessary to calculate the surface-pressure distribution on a wing-body configuration and to estimate the viscous drag for the condition of an all-turbulent boundary layer. For the purposes of obtaining the viscous drag, the body alone and the wing alone were considered to be in the free-stream flow with an all-turbulent boundary layer, no heat transfer, and a Prandtl number of unity. The friction drag on the body was obtained from the estimated boundary-layer growth on a body of revolution with pressure gradient by using the Von Kármán momentum equation as described in reference 4. The wings are assumed to be flat-plate surfaces with no pressure gradient, and the reference-temperature method of reference 9 is used in conjunction with the Prandtl-Schlichting incompressible skin-friction law to obtain the friction drag.

The computer program used to calculate the lifting solution is referred to as the MISLIFT program. The MISLIFT program includes the procedure necessary to calculate the lifting-pressure distribution over the configuration planform. The program then integrates these lifting pressures to provide force and moment effects at small angles of attack.

Both the MISDRAG and MISLIFT programs are available at a nominal fee through the following organization:

Computer Software Management Information Center (COSMIC)
Barrow Hall, University of Georgia
Athens, Georgia 30601

The MISDRAG program should be requested through COSMIC by the designation MISDRAG-LAR 10935; and the MISLIFT program, by MISLIFT-LAR 10932.

EXPERIMENT

An experimental program was conducted to provide surface-pressure data on a series of wing-body combinations. The tests were designed to provide basic data for the purpose of evaluating the theoretical methods described in the previous sections. In addition to the surface-pressure data provided for selected points on the configurations, the longitudinal forces and moments were obtained for each model of the series.

Apparatus and Tests

Tests were conducted in the high Mach number test section of the Langley Unitary Plan wind tunnel at Mach numbers of 2.5, 2.96, 3.95, and 4.5. Pressure data were taken at selected points on the wing and body surface at angles of attack from -6° to 6° . The slopes of the curves of the experimental pressure differential (lower-surface pressure minus upper-surface pressure) as a function of angle of attack $\frac{\Delta C_p}{\alpha}$ were obtained from the difference of the measured pressures at angles of attack of 2° and -2° .

The models were equipped with internally mounted strain-gage balances, and force and moment data were taken for an angle-of-attack range from -4° to 10° . For comparison with the theoretical methods the values of $\frac{x_{cp}}{l}$ and $C_{N\alpha}$ were obtained from the slopes of the curves of C_m and C_N against α at $\alpha = 0^{\circ}$. The zero-lift drag data presented have been adjusted so that the pressure on the base of the model is equal to free-stream static pressure. Boundary-layer transition was induced for the force tests by a strip of roughness particles near the leading edge of the wings and the nose of the body. The effectiveness of these roughness particles was verified by limited sublimation tests.

The Reynolds number for the pressure and force tests was 9.84×10^6 per meter (3.00×10^6 per foot). The other conditions for these tests are given in the following table:

Mach number	Stagnation temperature		Stagnation pressure	
	K	°F	kN/m ²	lbf/ft ²
2.5	339	150	122.0	2547
2.96	339	150	155.8	3253
3.95	353	175	277.4	5794
4.50	353	175	357.5	7467

Models

The series of models used in the present investigation consisted of a circular-arc body of revolution with four sets of wings having identical diamond-shaped planforms. The wings were tested at two longitudinal positions on the body with thickness ratios of 5 and 10 percent for each position. The wing sets all have symmetrical diamond-shaped airfoils with the maximum thickness at the midchord position. Dimensional details of the models with wings in the forward and aft positions are shown in figure 3. The locations of the pressure orifices are also illustrated in figure 3. The wing orifices are located on a chordwise survey line at 58.3 percent of the semispan. The orifice locations are presented in tables I to V along with the measured pressure coefficients for the range of test conditions considered.

RESULTS AND DISCUSSION

Zero-Lift Solution

The theoretical method presented in the present paper has been used to estimate the surface pressures on each of the model configurations used in the experimental tests. The calculation of the surface pressures at the zero-lift conditions was accomplished with the use of the computing program presented in reference 5.

A comparison of the theoretical estimates and the experimental results of the surface pressures is presented in figure 4 for each of the configurations considered. Figure 4(a) includes the pressure distributions along the body vertical meridian and wing survey line for the wing-body combination with the 10-percent-thick wing in the aft position. The theoretical estimates and the experimental data along the body vertical meridian are generally in good agreement over the Mach number range shown. The agreement on the wing survey line is only fair, with the theoretical estimates being generally lower over both the forward and aft panels of the wing. It should be noted that the theoretical methods

were developed especially for configurations with thin wings. In order to evaluate the effects of wing thickness on the accuracy of the theoretical estimates, a comparison of the experiment and theory is made in figure 4(b) for the aft-wing configuration with a wing thickness ratio of 5 percent. As might be expected, the agreement between theory and experiment on the wing survey line improves as the wing thickness ratio decreases. However, the results shown in figure 4(b) still indicate the theoretical estimates of the wing surface pressures to be generally lower than experiment.

The theoretical estimates of the surface pressures and the experimental values for the 10-percent-thick wing in the forward position are shown in figure 4(c). Along the vertical meridian on the body, the theoretical method overpredicts the wing interference effects on the body. Also, for the wing survey line, the theoretical method tends to overpredict the pressure on the forward part of the wing. These overprediction tendencies should be expected, since the assumption of thin wings in the presence of a low-fineness-ratio body is violated by the thick wings in the nose region. Indeed, for this configuration the wing is sufficiently thick at the wing-body juncture near the nose to produce essentially a blended wing-body effect.

The comparison of theory and experiment for the 5-percent-thick wing in the forward position is shown in figure 4(d). The results of figure 4(d) show some improvement of the agreement between theory and experiment for the thinner wing. However, the theoretical method still overpredicts the pressures on the forward portion of the wing, especially at the lower Mach numbers.

The data presented for comparison with theory have thus far been confined to surface pressures along body and wing survey lines. Axial-force data were obtained for each of the model configurations at zero-lift conditions and these data are presented in figure 5. The theoretical axial-force results presented in figure 5 represent the integrated surface pressure obtained by the present method coupled with a flat-plate skin analysis. Also included for comparison are the theoretical estimates of the axial force obtained from the supersonic-area-rule methods of reference 2.

The comparison of the present method with experimental data shown in figure 5 illustrates several important points. First, the agreement of the theoretical predictions is very good for the configurations with 5-percent-thick wings; however, as the wing thickness increases to 10 percent, the theory generally overpredicts the axial force. Second, the theoretical predictions for the body alone are in excellent agreement with experiment. Finally, the overall agreement of the present theoretical method indicates that reliable preliminary design estimates of the zero-lift axial force can be obtained from the present method for a class of configurations with relatively thin midwings and bodies of revolution having low fineness ratios.

Figure 5 indicates that the linear-theory methods of reference 2 show good agreement at the lower Mach numbers. As the Mach number increases, the agreement becomes

poor for the wing-forward configuration. It should be pointed out that the combination of configuration bluntness and Mach number for these conditions violates the basic linearity assumptions of the method of reference 2, and good agreement should not be expected.

Lifting Solutions

In order to evaluate the theoretical methods, estimates of the surface pressures induced by lifting conditions were made for the configurations represented by the series of experimental models. The comparisons of the theoretical estimates of the lifting pressures $\frac{\Delta C_p}{\alpha}$ with experimental values are made in figure 6. In figure 6, the lifting-pressure effects are shown along the body vertical meridian and along a chordwise survey line on the wing. The theoretical estimates are represented by the shaded bars. The oscillations of the estimated pressure distributions shown in figure 6 are inherent in the present numerical method and the method of reference 8. However, for the results presented in reference 8, a smoothing technique was used.

In figure 6(a) the theoretical estimates and the experimental values for the wing in the aft position are in good agreement along the body vertical meridian. It is significant to note that the theoretical estimates of the wing carryover lift (indicated by the pressure rise on the aft portion of the body) are also in good agreement with the experimental data. The comparison of the experiment and theory for the chordwise survey line on the wing indicates that the theoretical method tends to underpredict the lift pressures on the forward panel of the wing, especially at the lower Mach numbers.

The theoretical methods were applied to the model configuration with the 5- and 10-percent-thick wings in the forward position, and a comparison of these results with experiment is shown in figure 6(b). The oscillations of the theoretical method are large on the body survey line. However, it is evident that the mean variation of the theoretical estimate agrees well with the experimental data. The theoretical and experimental pressures on the wing survey line are also presented in figure 6(b), and the agreement is good at the higher Mach numbers and over the aft portion of the wing at lower Mach numbers.

Since the comparison of the estimates of lifting pressures with experiment are limited to two survey stations, it is in order to evaluate the theoretical methods in terms of the force and center-of-pressure characteristics of the entire configuration. The experimental normal-force characteristics and the centers of pressure at zero angle of attack are presented in figure 7 for the series of wing-body models considered in the present investigation. Theoretical estimates of the lifting characteristics shown in figure 7 are based on the present method of obtaining the lifting-pressure distribution and on the method presented in reference 2. The present method is generally in good agreement with the experimental values for all the configurations considered. It appears from the results shown in figure 7 that the present theoretical method can predict the value of the

normal-force slope within about 10 percent and the center of pressure within about 5 percent of the body length. These results indicate that the present method provides reliable preliminary design estimates for the detailed lift loading and overall lift characteristics of a class of configurations with thin wings and low-fineness-ratio bodies of revolution.

The comparison of the method of reference 2 with experiment shown in figure 7 indicates generally good results with the exception of the normal-force slope for the wing-aft configuration and the center of pressure for the body alone. The method of reference 2 assumes a mathematical model of the configuration to be a flat plate with the same planform as the configuration. This assumption is seriously violated by any configuration where the body claims a large portion of the planform area. Therefore, for the method of reference 2, good agreement should not be expected for configurations with small wings relative to the body size.

It should be pointed out that the present theoretical methods are not limited to the geometry of simple wing-body configurations. Indeed, any number of in-line lifting surfaces can be considered simultaneously. These surfaces can have small amounts of twist and camber or control deflection. For example, the basic method can be applied to provide estimates of fin and body loads for an in-line canard-wing-tail configuration. In addition to these loads, aerodynamic stability and control derivatives can be obtained for the complete configuration within the linear range.

CONCLUDING REMARKS

A theoretical method has been developed for estimating the aerodynamic loading on wing-body configurations at supersonic speeds and small angles of attack. In order to provide a basis for evaluation of the theoretical method, experimental measurements of surface pressure were made at selected survey positions on each of a series of basic wing-body configurations over a Mach number range from 2.5 to 4.5 and at angles of attack up to 6°. Force and moment measurements were also made for this same series of models at these test conditions. Comparison of the theoretical estimates with the experimental data generally indicated good agreement for the entire range of configuration and test variables. The agreement demonstrated by this comparison indicates that reliable preliminary design estimates can be obtained for the detailed aerodynamic loading as well as the longitudinal aerodynamic stability and control of complete wing-body configurations.

Langley Research Center,
National Aeronautics and Space Administration,
Hampton, Va., July 22, 1971.

REFERENCES

1. Pitts, William C.; Nielsen, Jack N.; and Kaattari, George E.: Lift and Center of Pressure of Wing-Body-Tail Combinations at Subsonic, Transonic, and Supersonic Speeds. NACA Rep. 1307, 1957.
2. Baals, Donald D.; Robins, A Warner; and Harris, Roy V., Jr.: Aerodynamic Design Integration of Supersonic Aircraft. AIAA Paper No. 68-1018, Oct. 1968.
3. Carmichael, Ralph L.; and Woodward, Frank A.: An Integrated Approach to the Analysis and Design of Wings and Wing-Body Combinations in Supersonic Flow. NASA TN D-3685, 1966.
4. Jackson, Charlie M., Jr.; and Smith, Rudeen S.: A Method for Determining the Total Drag of a Pointed Body of Revolution in Supersonic Flow With Turbulent Boundary Layer. NASA TN D-5046, 1969.
5. Jackson, Charlie M., Jr.; Sawyer, Wallace C.; and Smith, Rudeen S.: Estimation of Zero-Lift Drag of Missile Configurations in Supersonic Flow With Turbulent Boundary Layer. NASA TM X-1890, 1969.
6. Syvertson, Clarence A.; and Dennis, David H.: A Second-Order Shock-Expansion Method Applicable to Bodies of Revolution Near Zero Lift. NACA Rep. 1328, 1957. (Supersedes NACA TN 3527.)
7. Jones, Robert T.: Thin Oblique Airfoils at Supersonic Speed. NACA Rep. 851, 1946. (Supersedes NACA TN 1107.)
8. Middleton, Wilbur D.; and Carlson, Harry W.: A Numerical Method For Calculating the Flat-Plate Pressure Distributions on Supersonic Wings of Arbitrary Planform. NASA TN D-2570, 1965.
9. Sommer, Simon C.; and Short, Barbara J.: Free-Flight Measurements of Skin Friction of Turbulent Boundary Layers With High Rates of Heat Transfer at High Supersonic Speeds. J. Aeronaut. Sci., vol. 23, no. 6, June 1956, pp. 536-542.

TABLE II.- EXPERIMENTAL SURFACE PRESSURE COEFFICIENTS ON THE BODY WITH WING FORWARD, $t/c = 0.10$ (a) $M = 2.50$

Orifice number	Body orifice location, x/l	C_p at α of -					
		-6°	-4°	-2°	0°	2°	4°
1	.02857	.2023	.1650	.1345	.1070	.0809	.0552
2	.07142	.1913	.1569	.1250	.0989	.0706	.0471
3	.11428	.1780	.1444	.1140	.0864	.0596	.0390
4	.15714	.1619	.1297	.0985	.0709	.0493	.0273
5	.20000	.1494	.1157	.0868	.0621	.0405	.0207
6	.24285	.1339	.1032	.0735	.0518	.0302	.0111
7	.28571	.1185	.0885	.0625	.0408	.0191	.0015
8	.32857	.1045	.0775	.0515	.0297	.0103	-.0058
9	.37142	.0979	.0701	.0456	.0246	.0059	-.0110
10	.41428	.0920	.0657	.0434	.0246	.0066	-.0102
11	.45714	.0626	.0392	.0177	-.0012	-.0183	-.0323
12	.50000	.0391	.0186	.0022	.0196	.0360	-.0499
13	.54285	.0192	-.0012	-.0220	-.0365	-.0514	-.0639
14	.58571	.0119	-.0099	-.0274	-.0430	-.0575	-.0681
15	.62857	-.0051	-.0240	-.0406	-.0554	-.0683	-.0790
16	.67142	-.0168	-.0355	-.0512	-.0639	-.0769	-.0875
17	.71428	-.0277	-.0449	-.0588	-.0701	-.0745	-.0676
18	.75714	-.0379	-.0510	-.0576	-.0530	-.0404	-.0324
19	.80000	-.0409	-.0672	-.0447	-.0357	-.0301	-.0265
20	.84285	-.0438	-.0460	-.0412	-.0334	-.0289	-.0253
21	.88571	-.0535	-.0522	-.0435	-.0317	-.0295	-.0256
22	.92857	-.0655	-.0581	-.0462	-.0360	-.0286	-.0259
23	.97142	-.2365	-.2365	-.2362	-.2365	-.2368	-.2362
Wing orifice location, x'/c							
26	.09086	.2038	.1709	.1382	.1026	.0699	-.0448
27	.18172	.1869	.1533	.1235	.0930	.0610	.0236
28	.27258	.1758	.1430	.1140	.0871	.0574	.0324
29	.36193	.1648	.1356	.1066	.0820	.0515	.0287
30	.45064	.1574	.1290	.0985	.0739	.0456	.0236
31	.54569	-.0347	-.0522	-.0688	-.0853	-.0899	-.1104
32	.63655	-.0426	-.0604	-.0773	-.0929	-.1066	-.1168
33	.72741	-.0403	-.0595	-.0770	-.0921	-.1063	-.1189
34	.81827	-.0186	-.0440	-.0670	-.0859	-.1007	-.1136
35	.90913	-.0045	-.0278	-.0488	-.0677	-.0848	-.0989

(b) $M = 2.96$

Orifice number	Body orifice location, x/l	C_p at α of -					
		-6°	-4°	-2°	0°	2°	4°
1	.02857	.1948	.1636	.1285	.1030	.0769	.0543
2	.07142	.1865	.1512	.1193	.0930	.0670	.0452
3	.11428	.1740	.1404	.1069	.0805	.0570	.0369
4	.15714	.1574	.1230	.0919	.0672	.0454	.0261
5	.20000	.1450	.1105	.0803	.0581	.0371	.0195
6	.24285	.1292	.0964	.0687	.0464	.0288	.0112
7	.28571	.1151	.0840	.0579	.0381	.0205	.0029
8	.32857	.1010	.0732	.0479	.0298	.0122	-.0046
9	.37142	.0935	.0658	.0429	.0232	.0055	-.0087
10	.41428	.0935	.0674	.0446	.0281	.0122	-.0004
11	.45714	.0678	.0434	.0197	.0032	-.0103	-.0237
12	.50000	.0495	.0268	.0055	-.0093	-.0227	-.0353
13	.54285	.0312	.0102	-.0086	-.0226	-.0352	-.0461
14	.58571	.0221	.0028	-.0144	-.0274	-.0403	-.0510
15	.62857	.0068	-.0105	-.0267	-.0386	-.0506	-.0603
16	.67142	-.0045	-.0211	-.0366	-.0479	-.0582	-.0676
17	.71428	-.0144	-.0304	-.0449	-.0552	-.0638	-.0705
18	.75714	-.0260	-.0404	-.0519	-.0572	-.0565	-.0437
19	.80000	-.0347	-.0453	-.0492	-.0443	-.0343	-.0301
20	.84285	-.0406	-.0453	-.0413	-.0330	-.0280	-.0251
21	.88571	-.0443	-.0440	-.0366	-.0297	-.0260	-.0231
22	.92857	-.0493	-.0450	-.0356	-.0284	-.0237	-.0208
23	.97142	.0625	.0591	.0506	.0486	.0543	.0661
Wing orifice location, x'/c							
26	.09086	.2039	.1710	.1368	.1055	.0836	-.0237
27	.18172	.1865	.1528	.1218	.0938	.0645	.0286
28	.27258	.1765	.1420	.1118	.0880	.0587	.0369
29	.36193	.1666	.1337	.1035	.0797	.0537	.0328
30	.45064	.1566	.1255	.0952	.0722	.0479	.0269
31	.54569	-.0111	-.0271	-.0429	-.0562	-.0685	-.0818
32	.63655	-.0221	-.0380	-.0539	-.0662	-.0784	-.0871
33	.72741	-.0221	-.0394	-.0552	-.0675	-.0794	-.0904
34	.81827	-.0168	-.0367	-.0539	-.0668	-.0791	-.0901
35	.90913	-.0028	-.0241	-.0433	-.0575	-.0715	-.0828

TABLE III. EXPERIMENTAL SURFACE PRESSURE COEFFICIENTS ON THE BODY WITH WING FORWARD, $t/c = 0.05$

 (a) $M = 2.50$

Orifice number	Body orifice location, x/l	C_p at α of -					
		-6°	-4°	-2°	0°	2°	4°
1	.02857	.2025	.1638	.1327	.1054	.0781	.0530
2	.07142	.1921	.1556	.1246	.0951	.0686	.0449
3	.11428	.1781	.1431	.1121	.0825	.0582	.0368
4	.15714	.1597	.1261	.0944	.0678	.0457	.0242
5	.22000	.1456	.1121	.0841	.0589	.0376	.0161
6	.24285	.1301	.0981	.0715	.0471	.0258	.0065
7	.28571	.1124	.0826	.0568	.0346	.0140	-.0030
8	.32857	.0984	.0694	.0457	.0228	.0051	-.0126
9	.37142	.0896	.0605	.0376	.0162	-.0022	-.0178
10	.41428	.0851	.0583	.0361	.0169	-.0000	-.0148
11	.45714	.0637	.0391	.0184	-.0008	-.0170	-.0318
12	.50000	.0504	.0281	.0066	-.0118	-.0280	-.0421
13	.54285	.0335	.0104	-.0088	-.0251	-.0398	-.0546
14	.58571	.0196	-.0023	-.0202	-.0366	-.0510	-.0634
15	.62857	.0045	-.0152	-.0319	-.0469	-.0604	-.0730
16	.67142	-.0055	-.0243	-.0398	-.0542	-.0680	-.0801
17	.71428	-.0149	-.0322	-.0471	-.0607	-.0880	-.0684
18	.75714	-.0252	-.0410	-.0515	-.0545	-.0475	-.0394
19	.80000	-.0358	-.0459	-.0489	-.0443	-.0381	-.0344
20	.84285	-.0467	-.0512	-.0498	-.0422	-.0372	-.0341
21	.88571	-.0594	-.0603	-.0530	-.04	-.0369	-.0326
22	.92857	-.0738	-.0659	-.0536	-.0422	-.0340	-.0294
23	.97142	-.0084	-.0081	-.0085	-.0082	-.0085	-.0086
Wing orifice location, x'/c							
26	.C9C86	.1774	.1431	.1099	.0722	.0169	-.0642
27	.18172	.1671	.1328	.1010	.0678	.0391	-.0443
28	.27258	.1508	.1180	.0900	.0619	.0339	-.0325
29	.36193	.1449	.1136	.0870	.0575	.0317	-.0156
30	.45064	.1353	.1055	.0782	.0538	.0258	-.0075
31	.54569	.0222	.0007	-.0193	-.0378	-.0534	-.0681
32	.63655	.0187	-.0037	-.0246	-.0434	-.0601	-.0751
33	.72741	.0146	-.0087	-.0301	-.0495	-.0639	-.0795
34	.81827	.0264	.0015	-.0208	-.0404	-.0569	-.0736
35	.90913	.0269	.0033	-.0178	-.0366	-.0542	-.0701

 (b) $M = 2.96$

Orifice number	Body orifice location, x/l	C_p at α of -					
		-6°	-4°	-2°	0°	2°	4°
1	.02857	.1961	.1617	.1293	.0992	.0722	.0496
2	.07142	.1877	.1500	.1193	.0883	.0622	.0405
3	.11428	.1727	.1375	.1067	.0775	.0539	.0330
4	.15714	.1543	.1208	.0925	.0649	.0413	.0230
5	.22000	.1410	.1083	.0792	.0541	.0330	.0163
6	.24285	.1243	.0924	.0666	.0440	.0247	.0063
7	.28571	.1067	.0782	.0541	.0324	.0147	-.0021
8	.32857	.0925	.0657	.0441	.0232	.0055	-.0096
9	.37142	.0825	.0565	.0357	.0165	-.0012	-.0162
10	.41428	.0833	.0607	.0407	.0232	.0080	-.0054
11	.45714	.0633	.0390	.0174	.0006	-.0145	-.0279
12	.50000	.0516	.0298	.0098	-.0077	-.0212	-.0346
13	.54285	.0382	.0164	-.0019	-.0177	-.0312	-.0421
14	.58571	.0255	.0060	-.0098	-.0247	-.0373	-.0480
15	.62857	.0122	-.0059	-.0207	-.0347	-.0459	-.0562
16	.67142	.0012	-.0159	-.0297	-.0420	-.0526	-.0625
17	.71428	-.0078	-.0239	-.0363	-.0479	-.0572	-.0659
18	.75714	-.0182	-.0319	-.0423	-.0509	-.0519	-.0476
19	.80000	-.0265	-.0376	-.0449	-.0470	-.0396	-.0344
20	.84285	-.0348	-.0429	-.0453	-.0403	-.0333	-.0307
21	.88571	-.0438	-.0475	-.0449	-.0370	-.0310	-.0277
22	.92857	-.0521	-.0519	-.0446	-.0350	-.0290	-.0241
23	.97142	.0854	.0859	.0861	.0861	.0861	.0857
Wing orifice location, x'/c							
26	.C9C86	.1760	.1408	.1076	.0716	.0021	-.0421
27	.18172	.1635	.1300	.1000	.0674	.0447	-.0363
28	.27258	.1485	.1158	.0884	.0608	.0363	-.0121
29	.36193	.1426	.1116	.0850	.0574	.0355	.0004
30	.45064	.1309	.1024	.0758	.0541	.0297	.0038
31	.54569	.0355	.0147	-.0035	-.0207	-.0357	-.0470
32	.63655	.0278	.0070	-.0108	-.0270	-.0423	-.0553
33	.72741	.0218	.0004	-.0171	-.0327	-.0469	-.0589
34	.81827	.0275	.0047	-.0134	-.0304	-.0443	-.0572
35	.90913	.0285	.0067	-.0108	-.0274	-.0423	-.0559

TABLE IV.- EXPERIMENTAL SURFACE PRESSURE COEFFICIENTS ON THE BODY WITH WING AFT, t/c = 0.10
 (a) M = 2.50

Orifice number	Body orifice location, x/l	C _p at α of -						
		-6°	-4°	-2°	0°	2°	4°	6°
1	.02857	.1831	.1518	.1266	.1021	.0807	.0616	.0458
2	.07142	.1668	.1378	.1125	.0880	.0674	.0498	.0340
3	.11428	.1543	.1244	.0992	.0755	.0548	.0409	.0281
4	.15714	.1344	.1059	.0814	.0592	.0430	.0320	.0192
5	.20000	.1204	.0919	.0688	.0503	.0363	.0239	.0118
6	.24285	.1019	.0763	.0563	.0385	.0252	.0136	.0037
7	.28571	.0849	.0608	.0430	.0266	.0141	.0040	-.0052
8	.32857	.0695	.0475	.0304	.0148	.0038	-.0041	-.0111
9	.37142	.0562	.0364	.0200	.0059	-.0014	-.0100	-.0163
10	.41428	.0510	.0327	.0193	.0067	-.0007	-.0071	-.0126
11	.45714	.0304	.0142	.0015	-.0118	-.0184	-.0219	-.0267
12	.50000	.0186	.0046	-.0074	-.0170	-.0236	-.0263	-.0296
13	.54285	.0090	-.0065	-.0162	-.0237	-.0288	-.0307	-.0326
14	.58571	-.0002	-.0127	-.0194	-.0265	-.0301	-.0300	-.0320
15	.62857	-.0111	-.0211	-.0285	-.0326	-.0328	-.0344	-.0381
16	.67142	-.0190	-.0273	-.0299	-.0313	-.0322	-.0382	-.0453
17	.71428	-.0016	-.0034	-.0111	-.0213	-.0287	-.0402	-.0514
18	.75714	.0530	.0289	.0088	-.0093	-.0246	-.0385	-.0538
19	.80000	.0294	.0084	-.0079	-.0206	-.0373	-.0491	-.0607
20	.84285	.0008	-.0169	-.0320	-.0472	-.0571	-.0675	-.0771
21	.88571	-.0237	-.0398	-.0542	-.06.5	-.0766	-.0859	-.0935
22	.92857	-.0425	-.0575	-.0713	-.0813	-.0909	-.0993	-.1065
23	.97142	-.0077	-.0068	-.0069	-.0069	-.0072	-.0071	-.0070
	Wing orifice location, x'/c							
26	.C5C86	.1631	.1289	.0933	.0555	.0200	-.0935	-.1398
27	.18172	.1469	.1141	.0799	.0444	.0089	-.0285	-.1051
28	.27258	.1351	.1030	.0718	.0400	.0045	-.0248	-.0725
29	.36193	.1307	.0993	.0674	.0400	.0045	-.0248	-.0614
30	.45064	.1233	.0919	.0615	.0340	.0038	-.0241	-.0540
31	.54569	-.0605	-.0797	-.0956	-.1097	-.1223	-.1341	-.1438
32	.63655	-.0646	-.0842	-.1005	-.1148	-.1299	-.1419	-.1527
33	.72741	-.0646	-.0839	-.1009	-.1148	-.1302	-.1433	-.1547
34	.81827	-.0622	-.0825	-.0998	-.1142	-.1292	-.1419	-.1527
35	.90913	-.0558	-.0780	-.0963	-.1121	-.1264	-.1382	-.1465

(b) M = 2.96

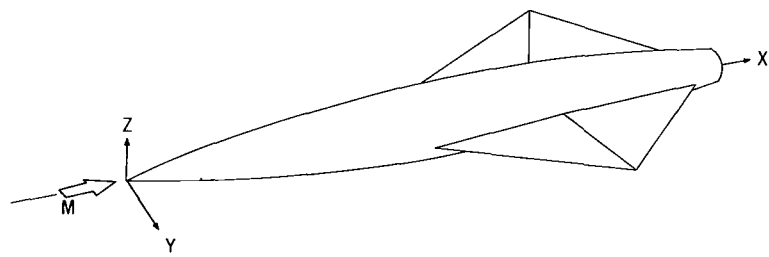
Orifice number	Body orifice location, x/l	C _p at α of -						
		-6°	-4°	-2°	0°	2°	4°	6°
1	.C2857	.1833	.1541	.1243	.1009	.0778	.0599	.0435
2	.07142	.1708	.1382	.1118	.0867	.0636	.0457	.0293
3	.11428	.1565	.1248	.0992	.0733	.0527	.0373	.0243
4	.15714	.1365	.1064	.0817	.0591	.0418	.0281	.0168
5	.20000	.1231	.0947	.0692	.0491	.0343	.0215	.0109
6	.24285	.1055	.0779	.0566	.0383	.0243	.0123	.0025
7	.28571	.0879	.0637	.0433	.0282	.0159	.0039	-.0050
8	.32857	.0729	.0503	.0332	.0182	.0059	-.0027	-.0100
9	.37142	.C5C95	.0394	.0241	.0107	-.0008	-.0086	-.0150
10	.41428	.0586	.0419	.0266	.0149	.0059	.0006	-.0050
11	.45714	.0361	.0194	.0057	-.0060	-.0142	-.0186	-.0234
12	.50000	.0252	.0102	-.0010	-.0102	-.0175	-.0219	-.0267
13	.54285	.C160	.0001	-.0094	-.0169	-.0234	-.0261	-.0292
14	.58571	-.0088	-.0034	-.0137	-.0201	-.0238	-.0260	-.0282
15	.62857	-.0012	-.0135	-.0222	-.0267	-.0288	-.0298	-.0328
16	.67142	-.0105	-.0216	-.0272	-.0294	-.0296	-.0333	-.0386
17	.71428	-.0117	-.0154	-.0180	-.0228	-.0276	-.0352	-.0433
18	.75714	.0332	.0175	.0026	-.0116	-.0238	-.0356	-.0471
19	.80000	.0270	.0101	-.0048	-.0170	-.0296	-.0406	-.0510
20	.84285	.C073	-.0073	-.0211	-.0313	-.0427	-.0518	-.0603
21	.88571	-.0102	-.0235	-.0361	-.0460	-.0563	-.0642	-.0715
22	.92857	-.0249	-.0370	-.0493	-.0587	-.0675	-.0754	-.0811
23	.97142	.0882	.0878	.0881	.0881	.0881	.0876	.0877
	Wing orifice location, x'/c							
26	.C5C86	.1632	.1273	.0951	.0600	.0209	-.0395	-.C911
27	.18172	.1473	.1147	.0800	.0474	.0109	-.0261	-.0803
28	.27258	.1339	.1014	.0717	.0416	.0092	-.0211	-.0644
29	.36193	.1298	.0963	.0667	.0391	.0067	-.0211	-.0543
30	.45064	.1231	.0905	.0616	.0341	.0059	-.0211	-.0501
31	.54569	-.0322	-.0490	-.0640	-.0773	-.0884	-.0993	-.1097
32	.63655	-.0415	-.0587	-.0741	-.0873	-.0992	-.1109	-.1209
33	.72741	-.0434	-.0610	-.0760	-.0893	-.1011	-.1129	-.1221
34	.81827	-.0442	-.0614	-.0760	-.0893	-.1011	-.1121	-.1202
35	.90913	-.0446	-.0618	-.0760	-.0889	-.1008	-.1090	-.1144

TABLE V.- EXPERIMENTAL SURFACE PRESSURE COEFFICIENTS ON THE BODY WITH WING AFT, $t/c = 0.05$ (a) $M = 2.50$

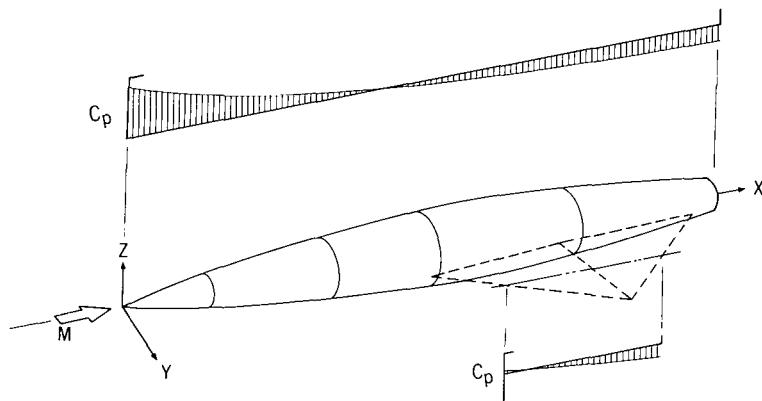
Orifice number	Body orifice location, x/l	C_p at α of -					
		-6°	-4°	-2°	0°	2°	4°
1	.C2857	.1854	.1497	.1262	.1017	.0805	.0610
2	.07142	.1679	.1362	.1138	.0888	.0675	.0497
3	.11428	.1538	.1226	.1002	.0758	.0557	.0418
4	.15714	.1358	.1046	.0816	.0606	.0432	.0322
5	.20000	.1205	.0916	.0697	.0499	.0370	.0237
6	.24285	.1036	.0758	.0573	.0392	.0263	.0136
7	.28571	.0861	.0606	.0443	.0273	.0134	.0040
8	.32857	.0698	.0471	.0307	.0161	.0043	-.0039
9	.37142	.0568	.0358	.0200	.0070	-.0019	-.0090
10	.41428	.0495	.0302	.0172	.0048	-.0024	-.0090
11	.45714	.0303	.0133	.0019	-.0099	-.0177	-.0220
12	.50000	.0202	.0048	-.0054	-.0166	-.0227	-.0254
13	.54285	.0094	-.0059	-.0156	-.0240	-.0272	-.0299
14	.58571	-.0007	-.0139	-.0203	-.0273	-.0306	-.0309
15	.62857	-.0114	-.0222	-.0293	-.0334	-.0345	-.0363
16	.67142	-.0201	-.0295	-.0325	-.0344	-.0379	-.0431
17	.71428	-.0192	-.0222	-.0264	-.0334	-.0413	-.0499
18	.75714	-.02371	-.0064	-.0196	-.0327	-.0438	-.0552
19	.80000	-.2368	-.0020	-.0183	-.0329	-.0467	-.0589
20	.84285	-.2380	-.0151	-.0298	-.0426	-.0567	-.0681
21	.88571	-.0104	-.0292	-.0437	-.0515	-.0695	-.0808
22	.92857	-.0209	-.0394	-.0544	-.0674	-.0793	-.0900
23	.97142	-.0092	-.0093	-.0088	-.0093	-.0095	-.0093
Wing orifice location, x'/c							
26	.C9C86	.1307	.0916	.0556	.0172	-.0532	-.1253
27	.18172	.1160	.0775	.0432	.0099	-.0227	-.0942
28	.27258	.1059	.0730	.0403	.0076	-.0239	-.0626
29	.36193	.0980	.0657	.0387	.0065	-.0239	-.0564
30	.45064	.0895	.0572	.0307	.0031	-.0250	-.0519
31	.54569	-.0145	-.0380	-.0568	-.0740	-.0931	-.1068
32	.63655	-.0160	-.0392	-.0585	-.0757	-.0960	-.1116
33	.72741	-.0158	-.0389	-.0588	-.0767	-.0956	-.1109
34	.81827	-.0128	-.0368	-.0571	-.0759	-.0934	-.1085
35	.9C913	-.0102	-.0341	-.0544	-.0740	-.0912	-.1060

(b) $M = 2.90$

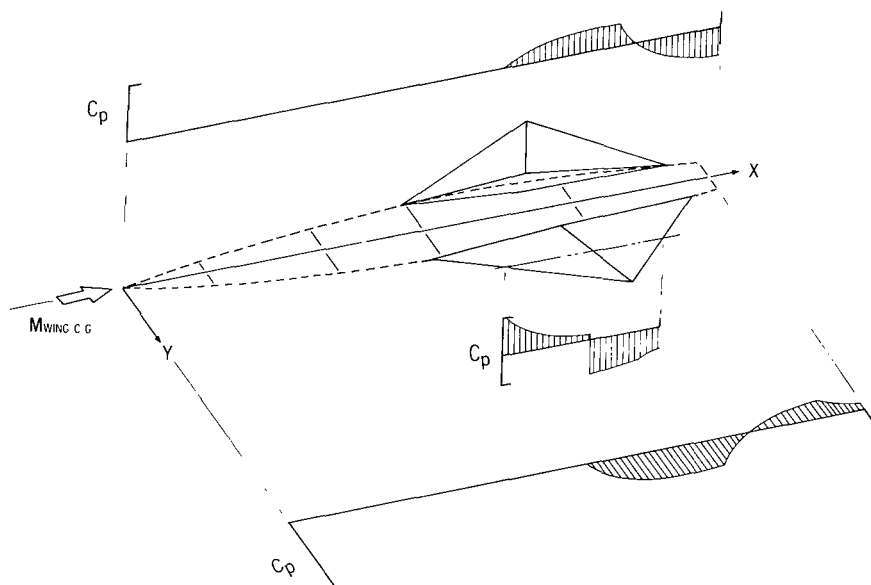
Orifice number	Body orifice location, x/l	C_p at α of -					
		-6°	-4°	-2°	0°	2°	4°
1	.C2857	.1814	.1517	.1233	.1000	.0777	.0579
2	.07142	.1692	.1371	.1106	.0859	.0649	.0457
3	.11428	.1559	.1250	.0978	.0732	.0534	.0368
4	.15714	.1374	.1065	.0806	.0585	.0419	.0285
5	.20000	.1240	.0931	.0691	.0489	.0343	.0215
6	.24285	.1074	.0778	.0563	.0374	.0247	.0125
7	.28571	.0902	.0638	.0429	.0285	.0151	.0042
8	.32857	.0749	.0511	.0327	.0170	.0062	-.0034
9	.37142	.0608	.0396	.0225	.0100	-.0002	-.0085
10	.41428	.0564	.0396	.0225	.0112	.0023	-.0034
11	.45714	.0372	.0211	.0047	-.0060	-.0123	-.0175
12	.50000	.0264	.0109	-.0011	-.0117	-.0175	-.0220
13	.54285	.0155	.0007	-.0093	-.0175	-.0226	-.0289
14	.58571	.0079	-.0044	-.0141	-.0204	-.0241	-.0283
15	.62857	-.0022	-.0143	-.0223	-.0267	-.0287	-.0307
16	.67142	-.0113	-.0223	-.0281	-.0306	-.0320	-.0356
17	.71428	-.0179	-.0245	-.0278	-.0308	-.0348	-.0409
18	.75714	-.0077	-.0146	-.0215	-.0297	-.0370	-.0458
19	.80000	.0115	-.0033	-.0168	-.0284	-.0386	-.0488
20	.84285	.0060	-.0093	-.0229	-.0339	-.0444	-.0544
21	.88571	-.0025	-.0184	-.0319	-.0429	-.0530	-.0623
22	.92857	-.0099	-.0256	-.0393	-.0509	-.0607	-.0700
23	.97142	.0849	.0850	.0849	.0846	.0849	.0847
Wing orifice location, x'/c							
26	.C9C86	.1297	.0938	.0583	.0227	-.0315	-.0775
27	.18172	.1150	.0785	.0455	.0151	-.0219	-.0724
28	.27258	.1048	.0727	.0404	.0106	-.0200	-.0641
29	.36193	.0978	.0670	.0378	.0087	-.0168	-.0488
30	.45064	.0908	.0593	.0327	.0061	-.0181	-.0437
31	.54569	.0022	-.0184	-.0369	-.0531	-.0697	-.0838
32	.63655	-.0022	-.0234	-.0424	-.0589	-.0763	-.0915
33	.72741	-.0041	-.0250	-.0435	-.0608	-.0772	-.1056
34	.81827	-.0052	-.0264	-.0448	-.0622	-.0766	-.0904
35	.9C913	-.0063	-.0272	-.0454	-.0622	-.0763	-.0890



(a) Example wing-body configuration.

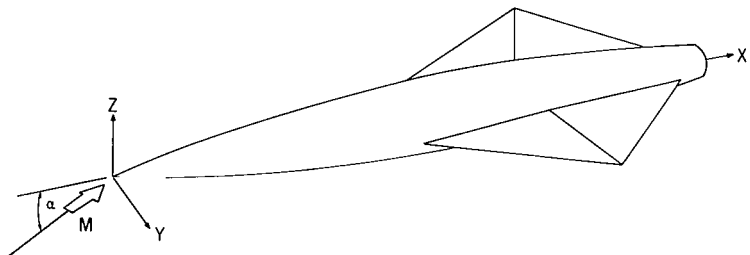


(b) Body-induced pressure fields.

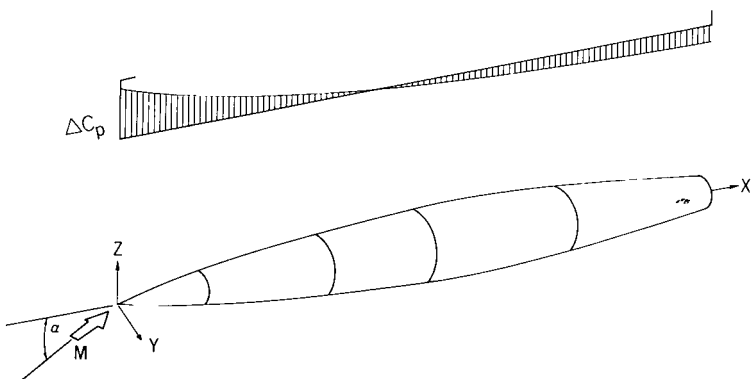


(c) Wing-induced pressure fields.

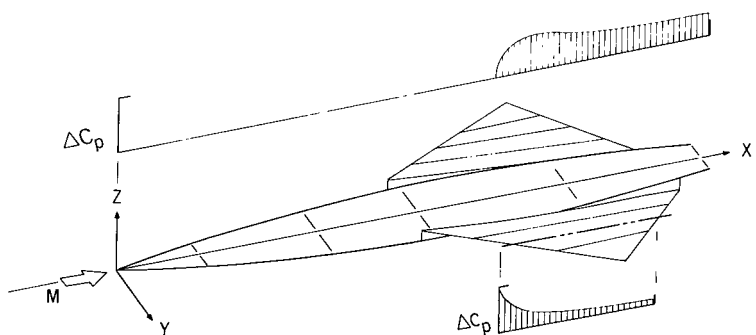
Figure 1.- Component pressure fields at zero lift.



(a) Example wing-body configuration.



(b) Body pressure field.



(c) Wing-induced pressure field.

Figure 2.- Component lifting-pressure fields.

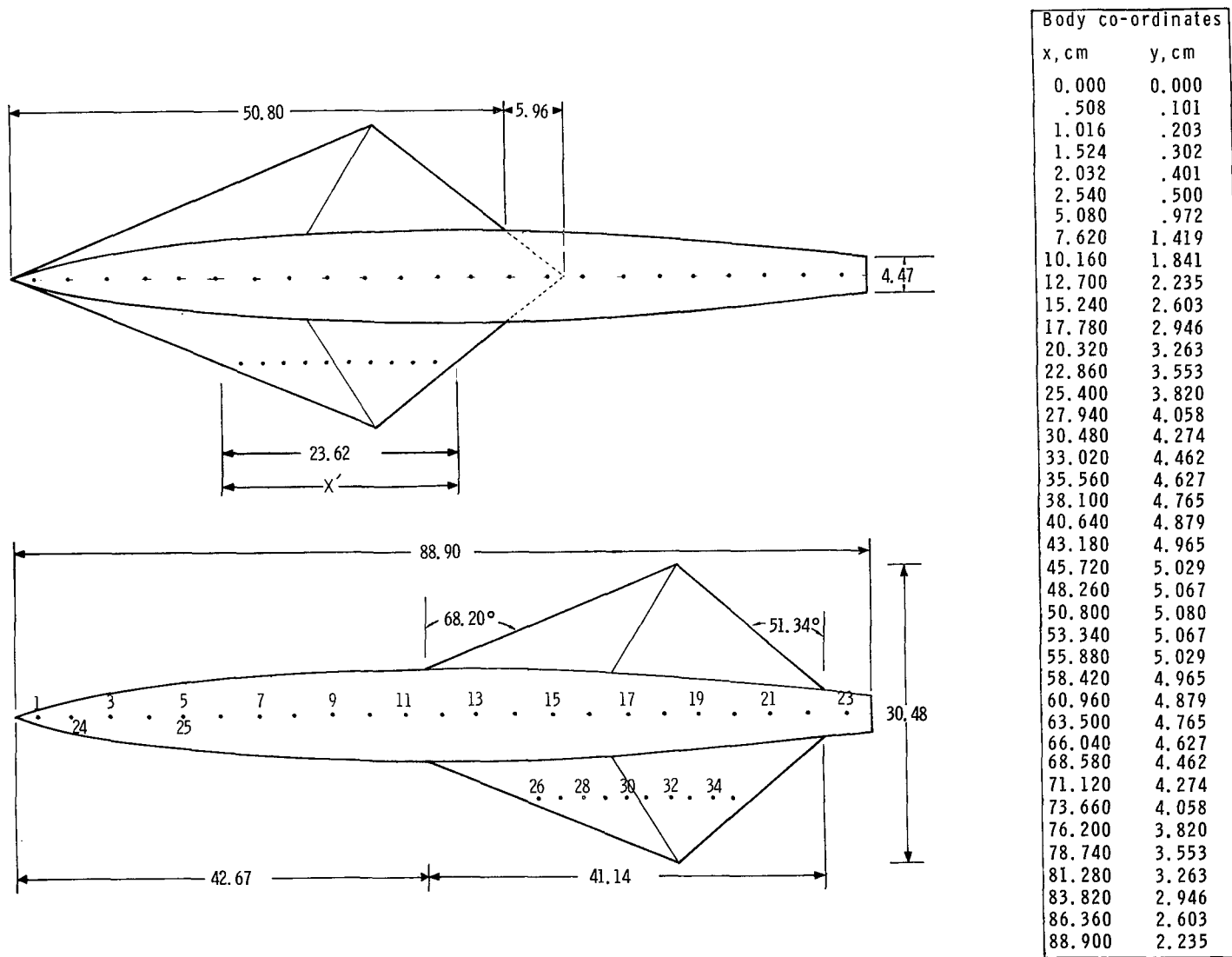
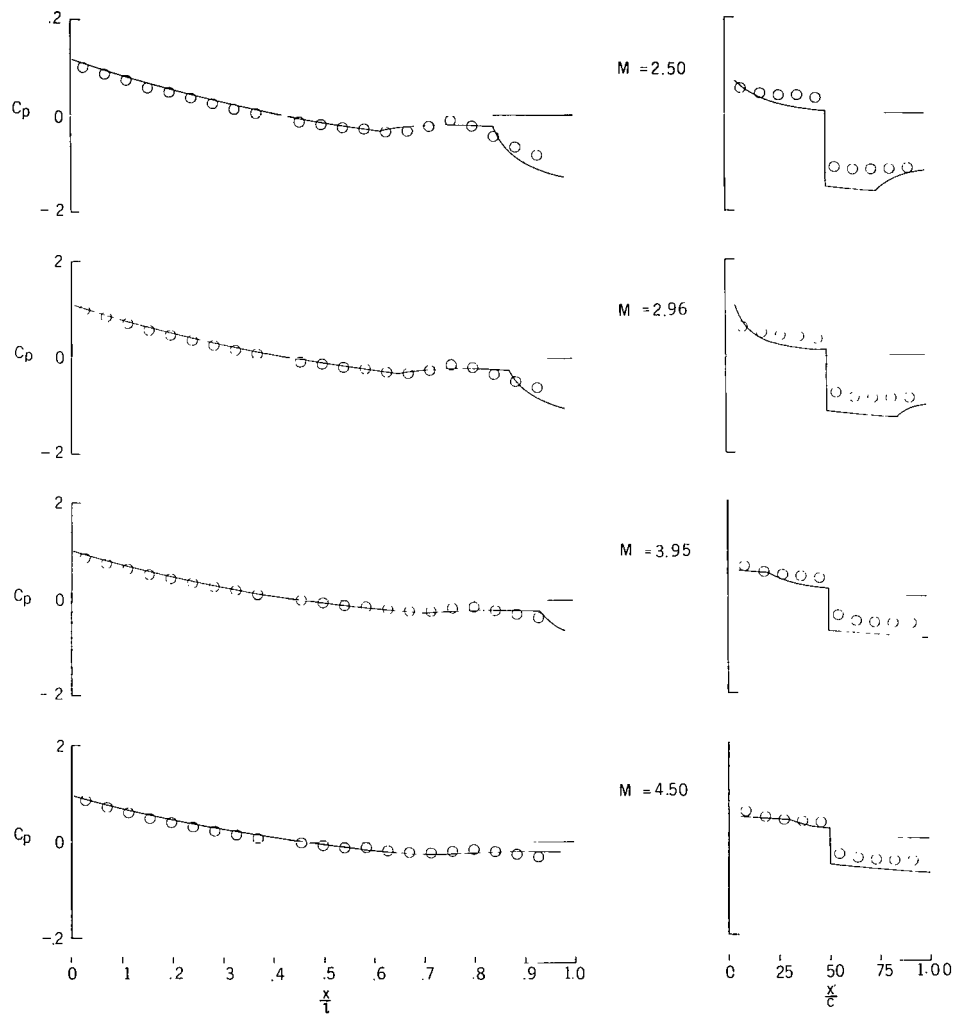
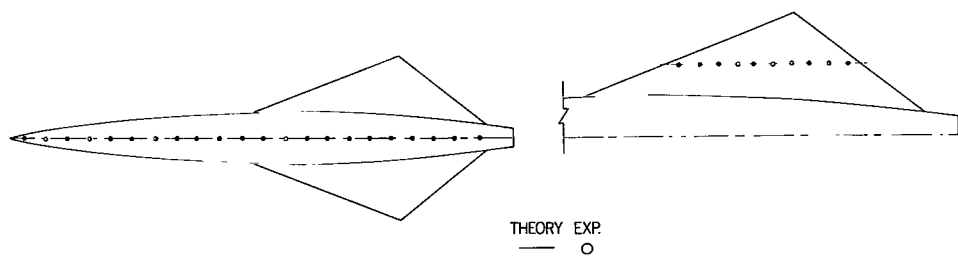
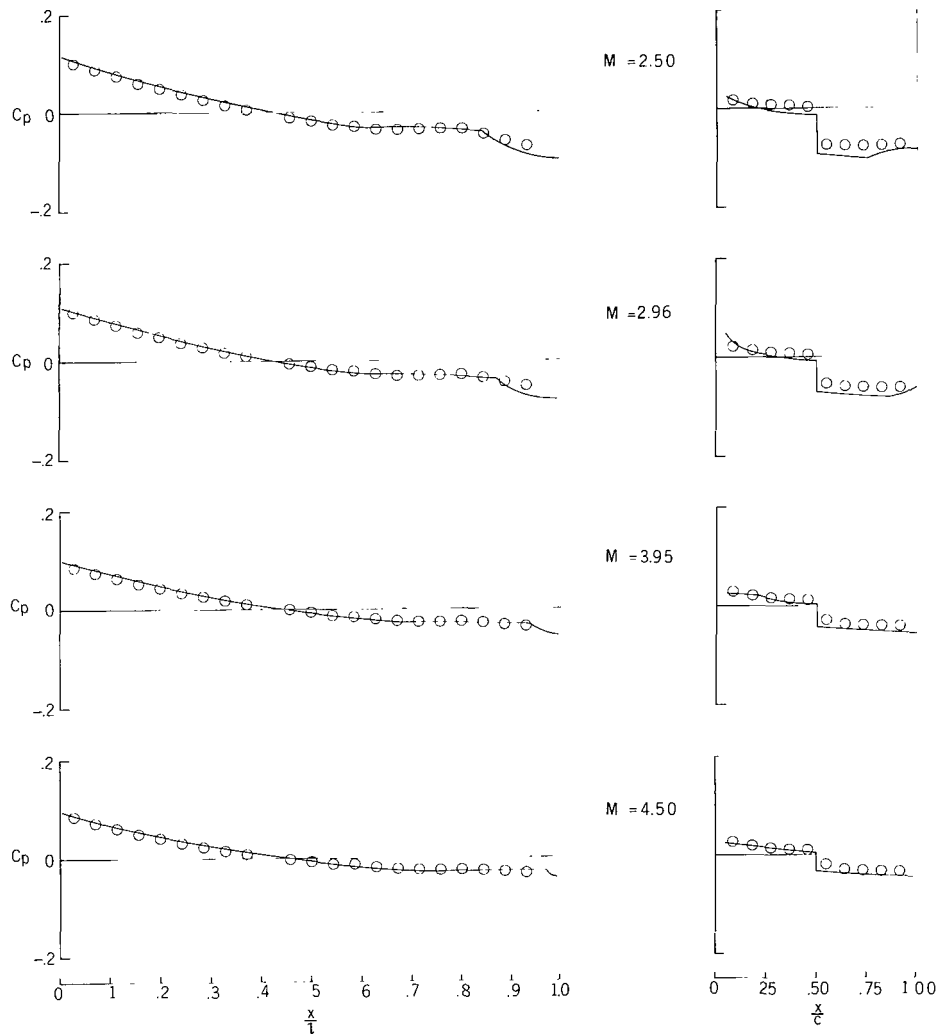
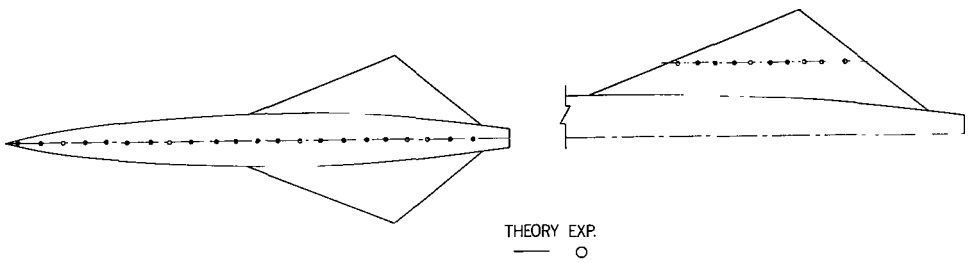


Figure 3.- Model details. (All dimensions are in cm. Numbers and dots denote pressure orifices.)



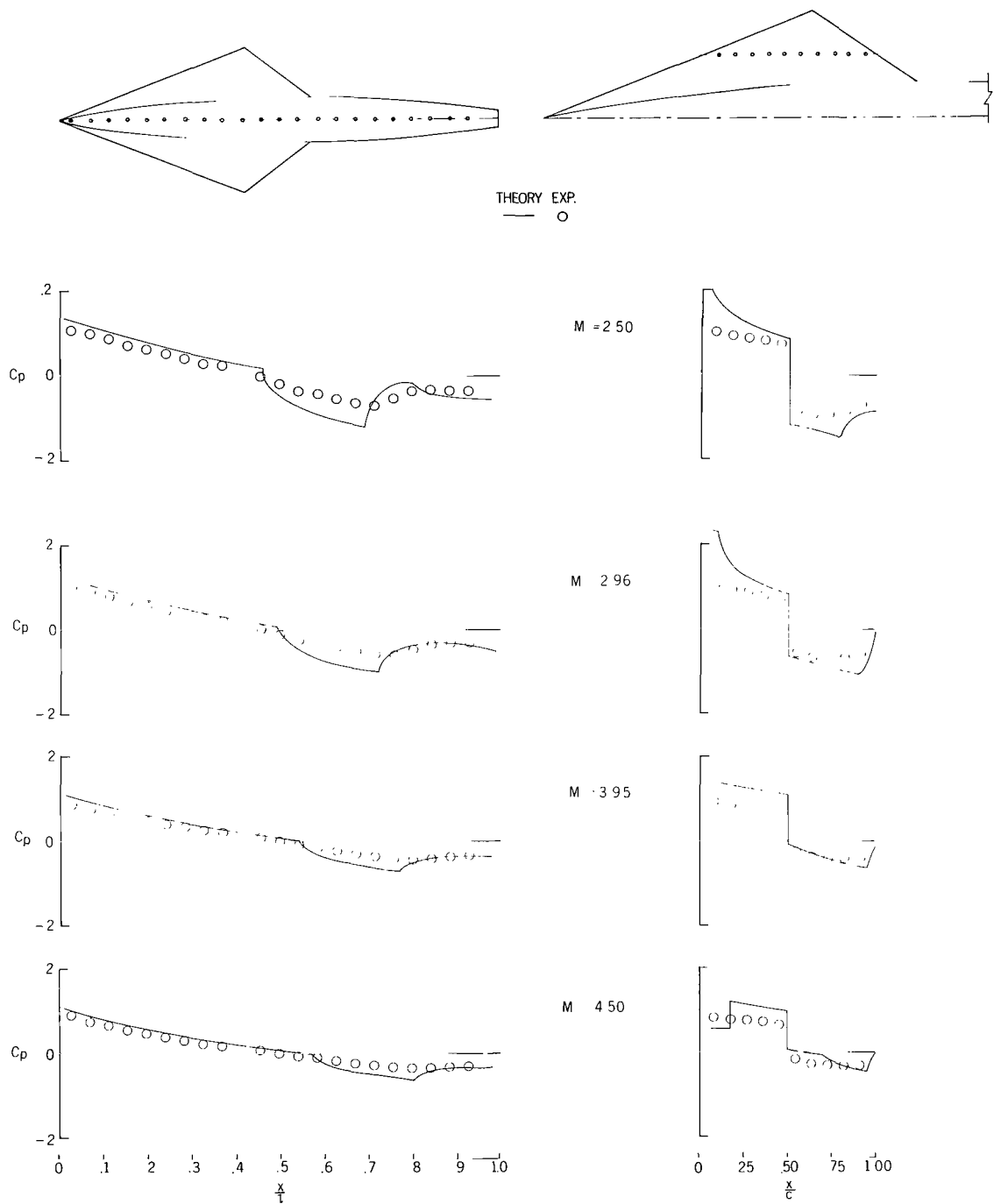
(a) Wing aft. $t/c = 0.10.$

Figure 4.- Comparison of experimental and theoretical surface pressures at zero-lift conditions.



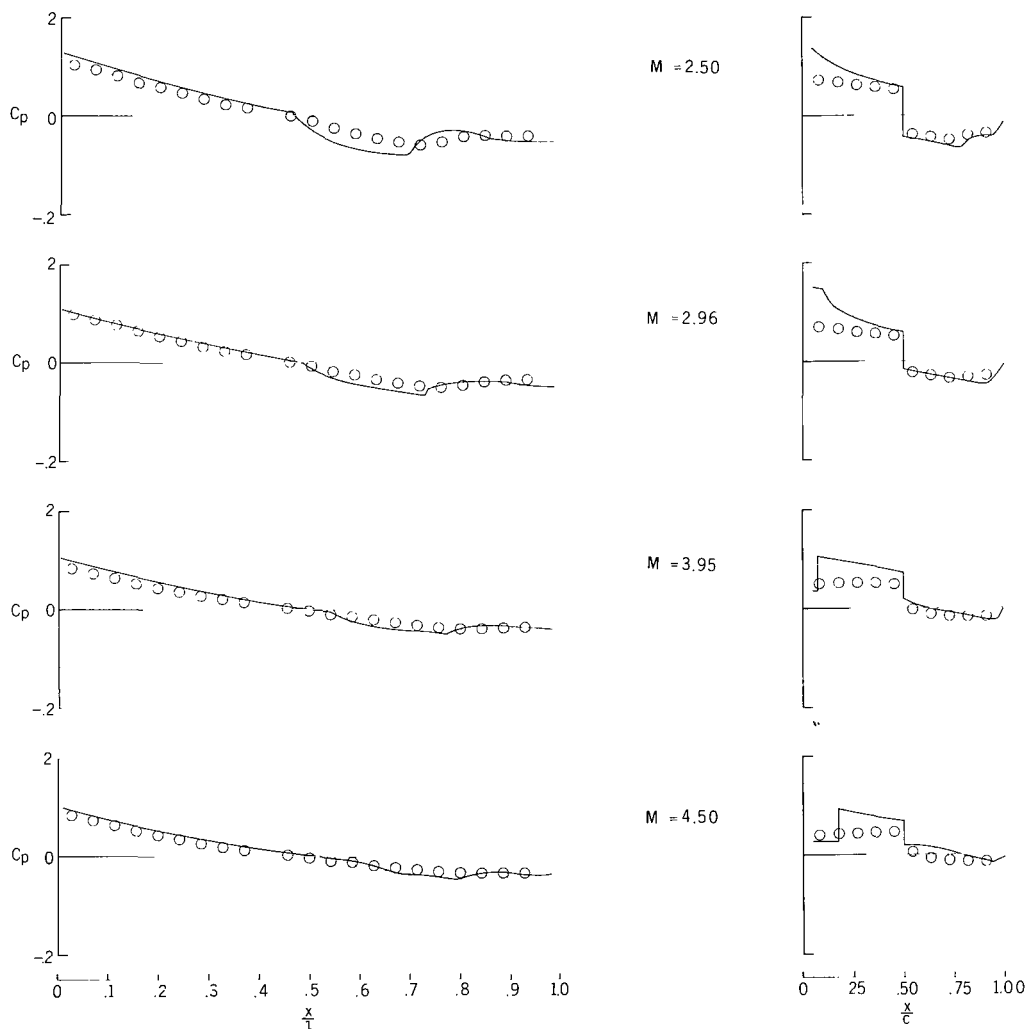
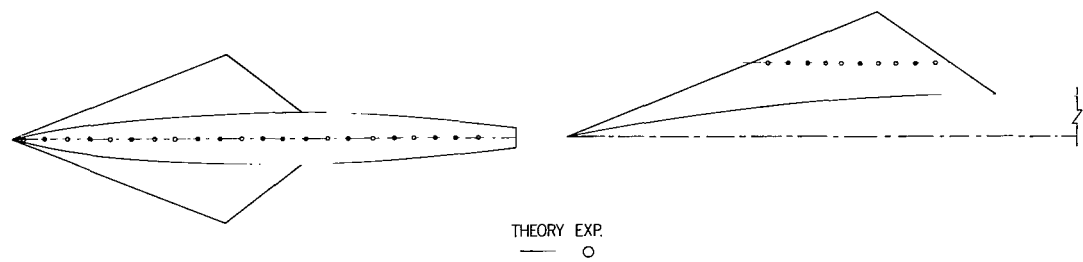
(b) Wing aft. $t/c = 0.05.$

Figure 4.- Continued.



(c) Wing forward. $t/c = 0.10.$

Figure 4-- Continued.



(d) Wing forward. $t/c = 0.05.$

Figure 4.- Concluded.

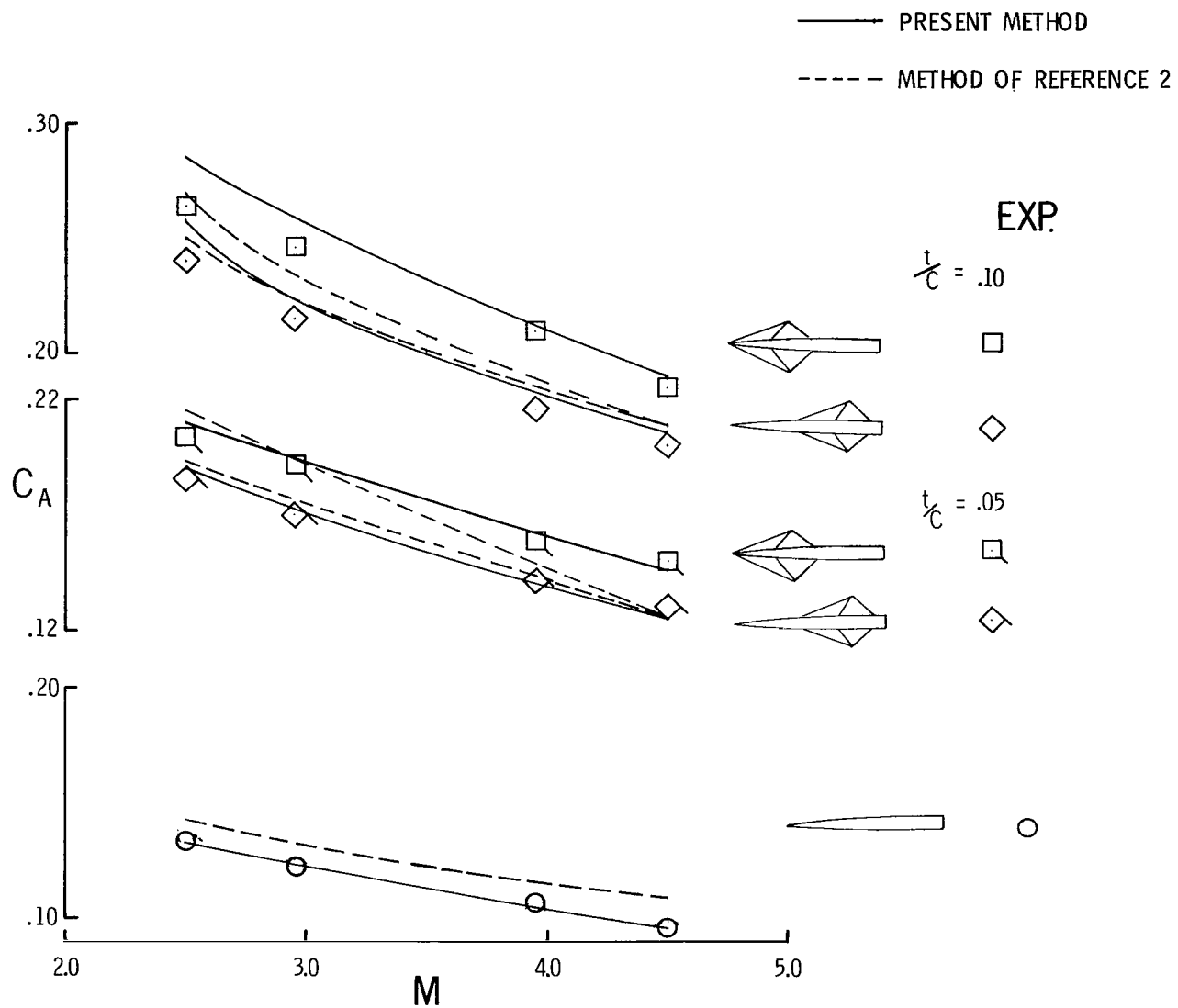
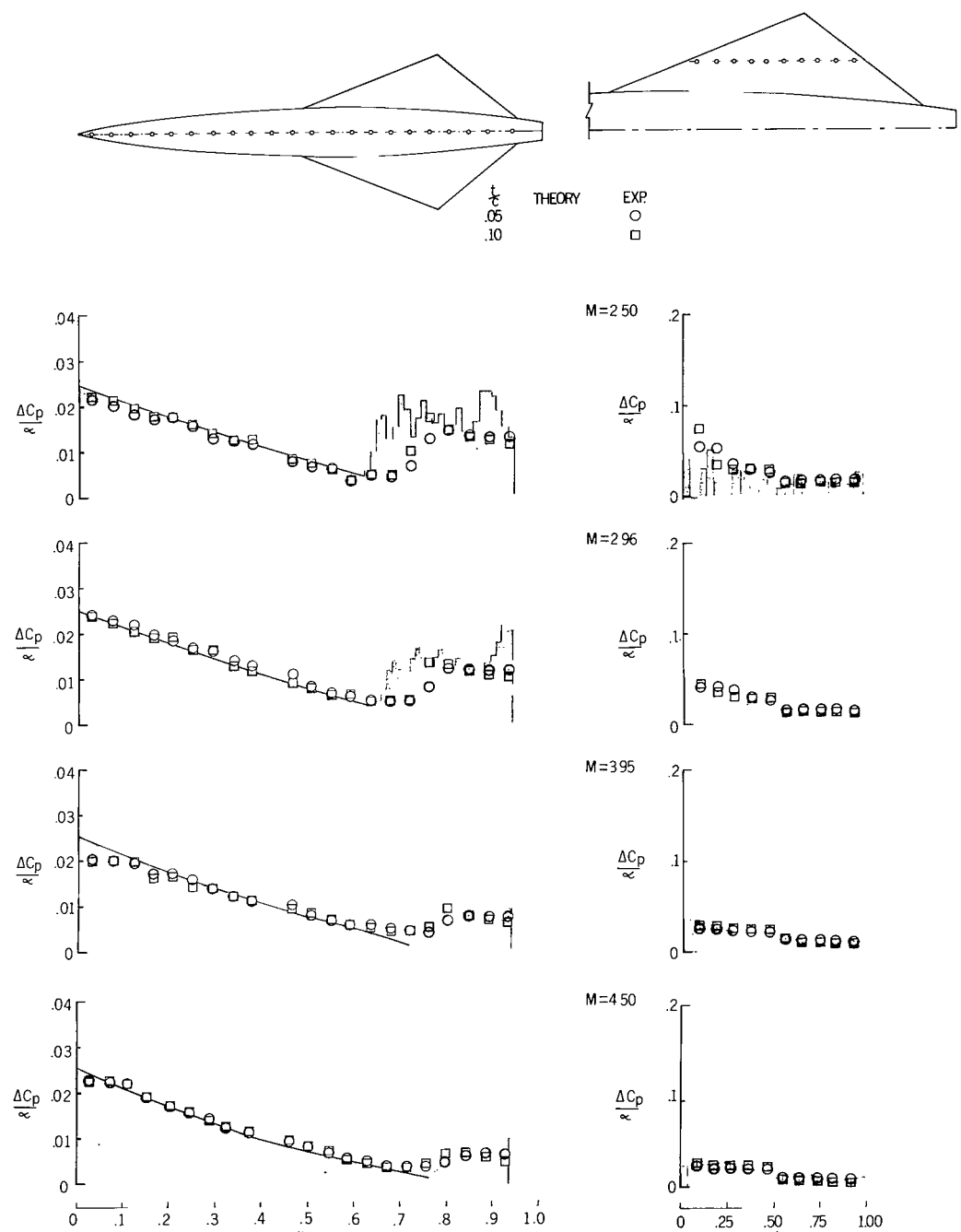
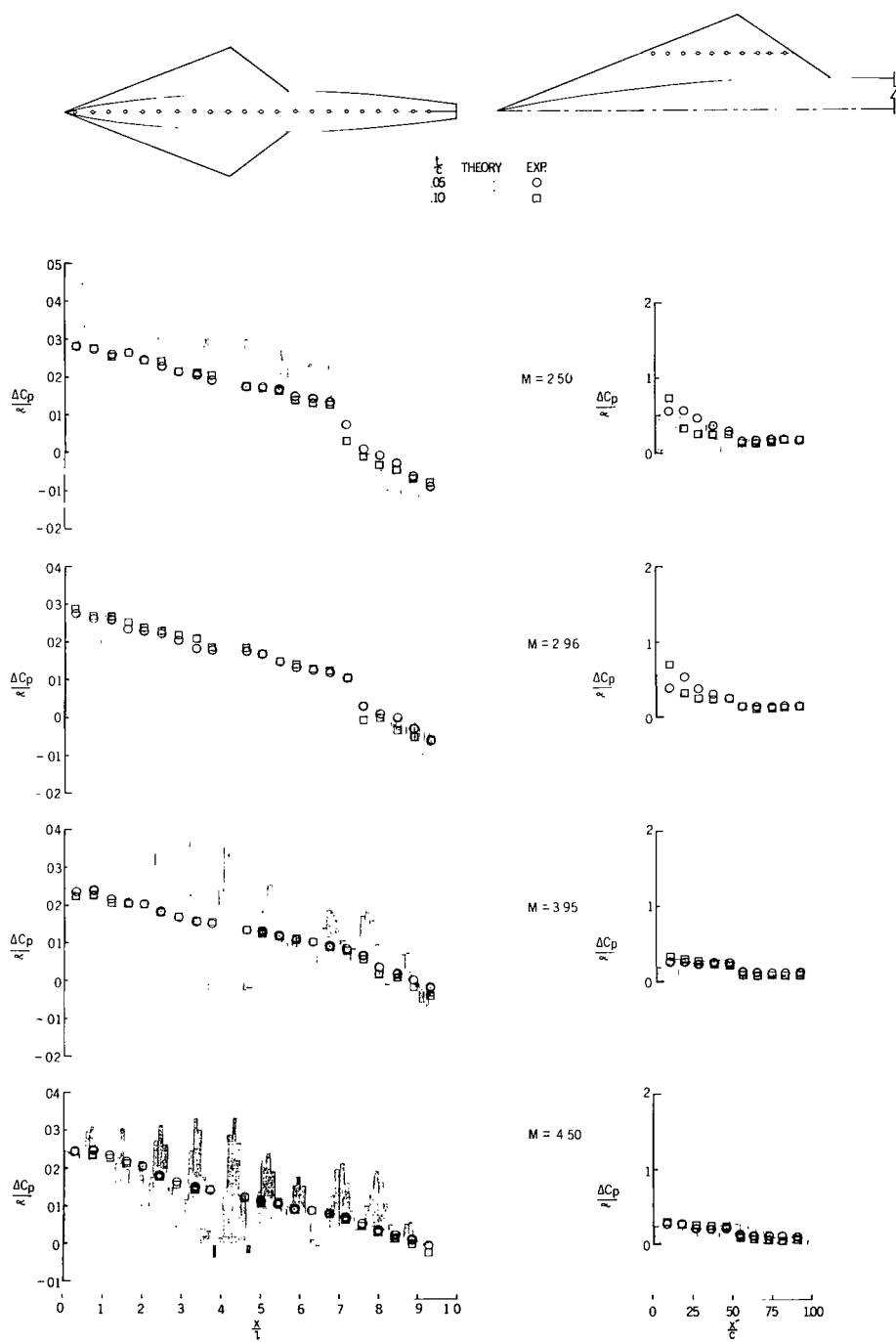


Figure 5.- Comparison of experimental and theoretical values for axial-force coefficients.



(a) Wing aft.

Figure 6.- Comparison of theoretical and experimental lifting pressures.



(b) Wing forward.

Figure 6.- Concluded.

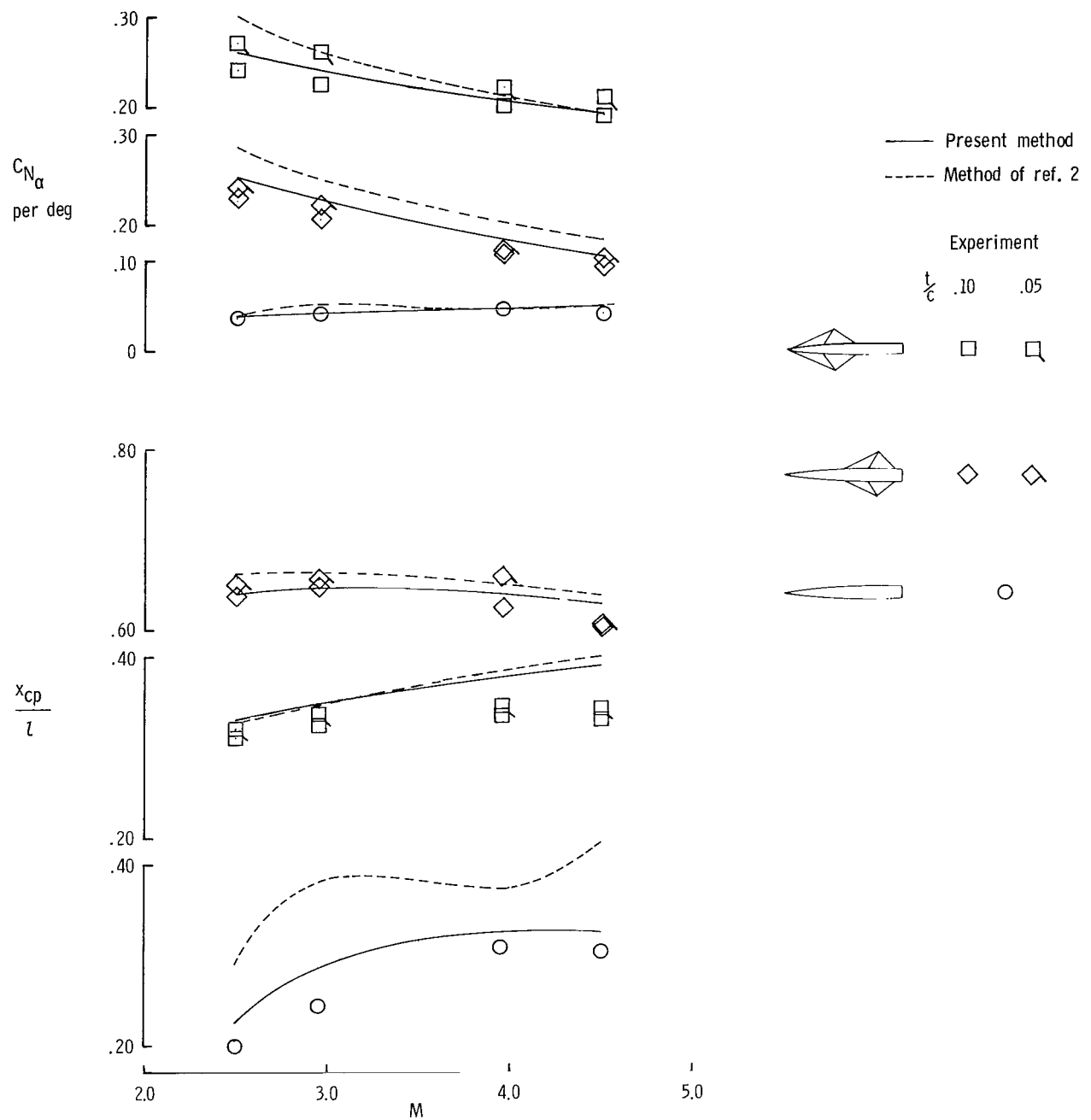


Figure 7.- Comparison of experimental and theoretical values of $C_{N\alpha}$ and x_{cp}/l .

NATIONAL AERONAUTICS AND SPACE ADMINISTRATION
WASHINGTON, D.C. 20546

OFFICIAL BUSINESS
PENALTY FOR PRIVATE USE \$300

FIRST CLASS MAIL

POSTAGE AND FEES PAID
NATIONAL AERONAUTICS AND
SPACE ADMINISTRATION



013 001 C1 U 01 711001 S00903DS
DEPT OF THE AIR FORCE
AF SYSTEMS COMMAND
AF WEAPONS LAB (WLOL)
ATTN: E LOU BOWMAN, CHIEF TECH LIBRARY
KIRTLAND AFB NM 87117

POSTMASTER: If Undeliverable (Section 158
Postal Manual) Do Not Return

"The aeronautical and space activities of the United States shall be conducted so as to contribute . . . to the expansion of human knowledge of phenomena in the atmosphere and space. The Administration shall provide for the widest practicable and appropriate dissemination of information concerning its activities and the results thereof."

— NATIONAL AERONAUTICS AND SPACE ACT OF 1958

NASA SCIENTIFIC AND TECHNICAL PUBLICATIONS

TECHNICAL REPORTS: Scientific and technical information considered important, complete, and a lasting contribution to existing knowledge.

TECHNICAL NOTES: Information less broad in scope but nevertheless of importance as a contribution to existing knowledge.

TECHNICAL MEMORANDUMS: Information receiving limited distribution because of preliminary data, security classification, or other reasons.

CONTRACTOR REPORTS: Scientific and technical information generated under a NASA contract or grant and considered an important contribution to existing knowledge.

TECHNICAL TRANSLATIONS: Information published in a foreign language considered to merit NASA distribution in English.

SPECIAL PUBLICATIONS: Information derived from or of value to NASA activities. Publications include conference proceedings, monographs, data compilations, handbooks, sourcebooks, and special bibliographies.

TECHNOLOGY UTILIZATION PUBLICATIONS: Information on technology used by NASA that may be of particular interest in commercial and other non-aerospace applications. Publications include Tech Briefs, Technology Utilization Reports and Technology Surveys.

Details on the availability of these publications may be obtained from:

SCIENTIFIC AND TECHNICAL INFORMATION OFFICE

NATIONAL AERONAUTICS AND SPACE ADMINISTRATION
Washington, D.C. 20546